Mechanism of Ethanol Reforming: Theoretical Foundations

Jeng-Han Wang,*,† C. S. Lee,‡ and M. C. Lin‡

Department of Chemistry, National Taiwan Normal University, Taipei, Taiwan, and Institute of Molecular Science and Department of Applied Chemistry, National Chiao Tung University, Hsinchu, Taiwan

Received: November 24, 2008; Revised Manuscript Received: February 11, 2009

The mechanism of ethanol reforming has been systematically studied by both energetic calculation to examine ethanol decomposition and electronic structure analysis to investigate the redox capability of the nine selected metals of Co, Ni, Cu, Rh, Pd, Ag, Ir, Pt, and Au with the same crystal structure and surface orientation. The energetic calculation shows that most of the dissociation barriers are lower on Co(111), Ni(111), Rh(111), and Ir(111) surfaces and higher on Cu(111), Ag(111), and Au(111) surfaces. The initial C−H bond dissociation, forming the doubly adsorbed *C(H_2)C(H_2)O(H)* and *C(H_2)C(H_2)O*, with a lower barrier than those in the initial C−C and C−O bond dissociations is considered as the most feasible decomposition route. In addition, the linear correlation between reaction barriers and d-band centers breaks down in the case of C−H bond dissociation due to the lower barriers on Rh(111) and Ir(111) surfaces. This result may be related to the suitable bond distances on Rh(111) and Ir(111) surfaces to form the more stable double adsorbates, *C(H_2)C(H_2)O(H)* and *C(H_2)C(H_2)O*. In the electronic structure analysis, Rh(111) and Ir(111) surfaces with higher density of state (DOS) distributions around the Fermi level can efficiently accept/donate electrons from/to the reacting ethanol and its fragments, showing better redox capability. Therefore, the excellent efficiency of Rh- and Ir-based catalysts, as observed from the reforming experiment, can be attributed to both the lower decomposition barrier and the higher DOS distribution around the Fermi level based on the first-principles calculation.

1. Introduction

The rising concern over global warming and the dwindling supply of oil reserves have led to the general public's awareness of the detrimental outcome from the world's addiction to fossil fuels and many governments' attention to research on the clean hydrogen fuel, which is considered as the primary fuel for future fuel cell application.[1] To make hydrogen fuel practically applicable, the main challenge lies in the development of viable technologies for economical hydrogen production, storage, and transportation. Among various approaches, the reforming of ethanol (i.e., conversion of ethanol to hydrogen) is expected to be an attractive one since ethanol is nontoxic with high hydrogen content, has a moderate production cost, is easy to handle, and is able to be produced from renewable biomass. Furthermore, the development of catalytic reformers with high stability and efficiency of hydrogen production is considered as the key technology in the reforming of ethanol. Therefore, a fundamental understanding of the mechanism of the reforming process will play a vital role in designing novel catalytic materials with high efficiencies, leading to a breakthrough in hydrogen economy.

In the reforming of ethanol, hydrogen can be obtained from the two main reactions, steam reforming and partial oxidation by reactions 1 and 2, respectively.

$$C_2H_5OH + 3H_2O \rightarrow 6H_2 + 2CO_2 \qquad \Delta H = 41.6\ \text{kcal/mol} \quad (1)$$

$$C_2H_5OH + \frac{3}{2}O_2 \rightarrow 3H_2 + 2CO_2 \qquad \Delta H = -132.0\ \text{kcal/mol} \quad (2)$$

In addition, cofeeding both steam and oxygen, ethanol can be reformed in an autothermal process in reaction 3

$$C_2H_5OH + 2H_2O + \frac{1}{2}O_2 \rightarrow 5H_2 + 2CO_2 \qquad \Delta H = -12.0\ \text{kcal/mol} \quad (3)$$

These reforming reactions have been extensively studied in various metal−metal oxide catalysts, including the metals of Co, Ni, Cu, Ru, Rh, Pd, Pt and Ir supported on the metal oxides of Al_2O_3, CeO_2, SiO_2, ZrO_2, TiO_2, MgO, La_2O_3, and Y_2O_3, as summarized in the recent reviews in refs 2−4. The result shows that the metals of Co, Ni, Ru, and Rh can help the carbon−carbon bond rupturing and the metal oxides of CeO_2 and La_2O_3 can enhance the oxidation process in the reforming of ethanol. Furthermore, Schmidt et al. have recently report the promising result of Rh/CeO_2 reformer,[5] in which ethanol−water mixture can be converted to hydrogen with the selectivity about 100% and the conversion efficiency over 95%. Their result demonstrates that ethanol can be efficiently converted to hydrogen with an appropriate catalyst and resolves the essential problem of the costly hydrogen production and transportation.

Furthermore, the mechanistic studies of ethanol adsorption and decomposition on numerous metal surfaces, Pt(111),[6−9] Ni(111),[10] Pd(111),[11] Rh(111),[12,13] and Au(111),[14] have been examined by first-principles calculations as well as by various experimental techniques, including X-ray photoelectron spectroscopy (XPS), IR spectroscopy, high resolution electron energy loss spectroscopy

* To whom correspondence should be addressed. Fax: (+886)2-2932-4249. E-mail: jenghan@ntnu.edu.tw.
† National Taiwan Normal University.
‡ National Chiao Tung University.

10.1021/jp810307h CCC: $40.75
Published on Web 03/26/2009

(HREELS), and temperature programmed desorption (TPD). These results show that ethanol can adsorb on the surface forming multilayer adsorbates at low temperatures and undergo dissociation and desorption at increasing surface temperature. The results[10,12,13] also show that Ni(111) and Rh(111) surfaces have better capabilities in decomposing the adsorbed ethanol than other metal surfaces. However, based on the decomposition result, the ethanol reforming mechanism is still not clear and the reforming activity cannot be rationally determined.

Herein, the detailed ethanol reforming mechanism has been thoroughly examined by the means of first-principles calculation. The decomposition and redox reactions, which have been considered as the key reactions in the reforming of ethanol,[2−4] are systematically studied on the surfaces of the 3d to 5d metals of the groups 9 (Co, Rh, and Ir), 10 (Ni, Pd, and Pt), and 11 (Cu, Ag, and Au) elements with the same crystal structures (face centered cubic, FCC) to minimize the geometrical effect in the catalytic reaction. In the decomposition reaction, from molecularly adsorbed ethanol to atomically adsorbed C, O, and H, the thorough potential energy surface (PES) has been elucidated by computing all the possible elementary steps of C−C, C−O, C−H, and O−H bond breaking processes. On the other hand, the redox capability of catalysts, which plays an important role in the reforming of ethanol as well, has been identified by analyzing electronic structures of catalytic materials. Comparing the activities of a series of metals for these two main reactions, the fundamental chemistry behind the catalytic ability can be thoroughly understood.

2. Computational Method

The calculations are performed using the Vienna ab initio Simulation Package (VASP),[15−17] at the density functional theory (DFT) level with a 3D periodic boundary condition. The exchange-correlation function is treated by the generalized gradient approximation (GGA)[18] with Perdew−Wang 1991 (PW91) formulation.[19] Combining the accuracy of augmented plane waves with the cost-effective pseudopotentials implemented in VASP, the projector-augmented wave method (PAW)[20,21] is applied in the basis set. The kinetic cutoff energy of 600 eV is employed and the Brillouin-zone (BZ) integration is sampled at about a 0.05 × 2 (1/Å) interval in the reciprocal space by the Monkhorst-Pack scheme.[22] Higher cutoff energies and *k*-point values with smaller BZ sampling intervals are applied to examine the convergence of current calculations. The spin effect is included in the case of ferromagnetic cobalt and nickel in the present calculation.

In the surface calculation, since the structural effect of surface defects, steps, kinks, or terraces could affect the dissociation barriers in catalytic reactions and the electronic structures of catalysts in a similar manner on the metals with the same crystal structures,[23−26] only the most stable (111) surface of the FCC catalysts has been employed. The (111) surface is modeled by a five-layer slab in a (4 × 4) surface unit cell to limit interaction among the ethanol dissociated species. An equivalent five-layer vacuum space between two consecutive metal slabs is introduced to minimize the interaction between the distinct slabs. The surface models with more slabs or larger vacuum spaces have been tested for convergence and show negligibly energetic differences in the molecular ethanol adsorption.

The adsorption structures and energies of interesting intermediates in ethanol decomposition reaction are optimized and computed with the bottom two layers of the modeled slab fixed at the computed lattice constants to represent the semi-infinite bulk crystal (beneath the surface) and the top three layers free to relax. The nudged elastic band (NEB) method,[27] applied by simultaneously relaxing an interpolated chain of configurations between the initial and final positions along the minimum energy pathway, is employed to locate transition states in the ethanol decomposition reaction. The computed reaction barriers are correlated with the d-band centers, the projected d-band density of states relative to the Fermi level, to obtain the correlation coefficients, R^2.

3. Results and Discussion

The decomposition starts from the molecularly adsorbed ethanol with the most stable adsorption structure on the atop site[8,13,28] and follows by the initial C−C, C−O, C−H, and O−H bond breaking processes, which lead to four possible routes in reactions 4−7, respectively.

$$C_2H_5O(H)^* \xrightarrow{TS(CC1)} H_3C^* + {}^*C(H_2)O(H)^* \xrightarrow{TS(CO1)} H_3C^* + H_2C^* + HO^* \quad (4)$$

$$C_2H_5O(H)^* \xrightarrow{TS(CO2)} H_3C(H_2)C^* + HO^* \xrightarrow{TS(CC2)} H_3C^* + H_2C^* + HO^* \quad (5)$$

$$C_2H_5O(H)^* \xrightarrow{TS(CH1)} {}^*C(H_2)C(H_2)O(H)^* + H^* \rightarrow \begin{cases} \xrightarrow{TS(CC3)} H_2C^* + {}^*C(H_2)O(H)^* + H^* \xrightarrow{TS(CO3)} 2H_2C^* + HO^* + H^* \\ \xrightarrow{TS(CO4)} {}^*C(H_2)C(H_2)^* + HO^* + H^* \xrightarrow{TS(CC4)} 2H_2C^* + HO^* + H^* \end{cases} \quad (6)$$

$$C_2H_5O(H)^* \xrightarrow{TS(OH1)} C_2H_5O^* + H^* \quad (7)$$

The dissociation barriers of the transition states [TS(CC#), TS(CO#), TS(CH#), and TS(OH#) for C−C, C−O, C−H, and O−H bond breaking processes, respectively] and the related heats of reaction are listed in Table 1. The corresponded PES and geometrical structures on Rh(111) surface, for example, are shown in Figure 1. It is worth noting that C_α−H bond dissociation forming $C(H_3)C(H)O(H)^* + H^*$ has a 1.0 eV higher barrier than that of TS(CH1) in C_β−H dissociation, and is not considered in the present calculation.[12]

In reaction 7, the dissociated fragment of $C_2H_5O^*$ can further dissociate to form H_3C^*, H_2C^*, O*, and H* following alike routes in reactions 8−10. The energetic results are listed in Table 2 and the corresponding PES and geometrical structures of Rh(111) system, for example, are shown in Figure 2.

$$C_2H_5O^* \xrightarrow{TS(CC5)} H_3C^* + {}^*C(H_2)O^* \xrightarrow{TS(CO5)} H_3C^* + H_2C^* + O^* \quad (8)$$

TABLE 1: Dissociation Barriers and Heats of Reaction in Parentheses (eV) of Ethanol Decomposition Processes on the Nine Metal (111) Surfaces

	Co	Rh	Ir	Ni	Pd	Pt	Cu	Ag	Au
Reaction 4: $C_2H_5O(H)^* \xrightarrow{TS(CC1)} H_3C^* + {}^*C(H_2)O(H)^* \xrightarrow{TS(CO1)} H_3C^* + H_2C^* + HO^*$									
TS(CC1)	2.66(1.01)	2.65(0.50)	2.02(0.39)	2.24(0.88)	2.70(0.71)	2.35(0.14)	3.34(1.48)	4.36(2.22)	4.04(1.50)
TS(CO1)	0.64(-0.77)	1.07(0.01)	0.87(0.00)	1.20(-0.43)	1.32(0.69)	0.94(0.87)	1.45(0.17)	2.84(1.15)	2.14(1.62)
Reaction 5: $C_2H_5O(H)^* \xrightarrow{TS(CO2)} H_3C(H_2)C^* + HO^* \xrightarrow{TS(CC2)} H_3C^* + H_2C^* + HO^*$									
TS(CO2)	1.02(-0.16)	1.76(0.20)	1.71(0.37)	1.46(0.10)	2.23(0.59)	1.93(0.36)	1.78(0.45)	2.93(1.35)	2.48(1.50)
TS(CC2)	1.30(0.17)	1.20 (0.38)	1.78(0.18)	1.30(0.45)	1.43 (1.09)	1.93(0.56)	1.87(1.41)	2.66(2.00)	2.06(1.63)
Reaction 6: $C_2H_5O(H)^* \xrightarrow{TS(CH1)} {}^*C(H_2)C(H_2)O(H)^* + H^* \longrightarrow \begin{cases} \xrightarrow{TS(CC3)} H_2C^* + {}^*C(H_2)O(H)^* + H^* \xrightarrow{TS(CO3)} 2H_2C^* + HO^* + H^* \\ \xrightarrow{TS(CO4)} {}^*C(H_2)C(H_2)^* + HO^* + H^* \xrightarrow{TS(CC4)} 2H_2C^* + HO^* + H^* \end{cases}$									
TS(CH1)	1.34(0.46)	0.52(0.45)	0.48(0.41)	1.46(0.51)	1.38(0.55)	1.41(0.40)	2.03(1.09)	3.09(1.90)	2.90(1.33)
TS(CC3)	0.63(0.32)	1.02(-0.03)	0.60(-0.17)	0.86(0.17)	0.87(0.35)	1.14(0.28)	2.08(1.24)	2.71(2.09)	2.33(1.63)
TS(CO3)	0.34(-1.03)	1.00(-0.11)	0.94(0.45)	0.27(-0.43)	1.24(0.64)	1.28(0.87)	1.16(0.06)	2.83(1.13)	2.12(1.54)
TS(CO4)	0.03(-0.88)	0.42(-0.69)	0.54(-0.42)	0.14(-0.73)	0.68(-0.27)	0.78(0.27)	1.59(-0.43)	2.13(-0.27)	1.91(0.65)
TS(CC4)	0.88(0.86)	0.99(0.82)	1.28(0.33)	1.04(1.02)	1.66(1.48)	2.01(0.33)	2.76(1.99)	3.45(2.92)	2.70(2.52)
Reaction 7: $C_2H_5O(H)^* \xrightarrow{TS(OH1)} C_2H_5O^* + H^*$									
TS(OH1)	0.44(-0.74)	0.58(-0.19)	0.69(0.21)	0.67(-0.58)	0.70(0.25)	0.99(0.55)	1.10(-0.10)	1.94(0.84)	1.45(1.32)

Dissociation barriers: > 0.5 | 0.5 ~ 1.0 | 1.0 ~ 1.5 | 1.5 ~ 2.0 | 2.0 ~ 2.5 | > 2.5 eV

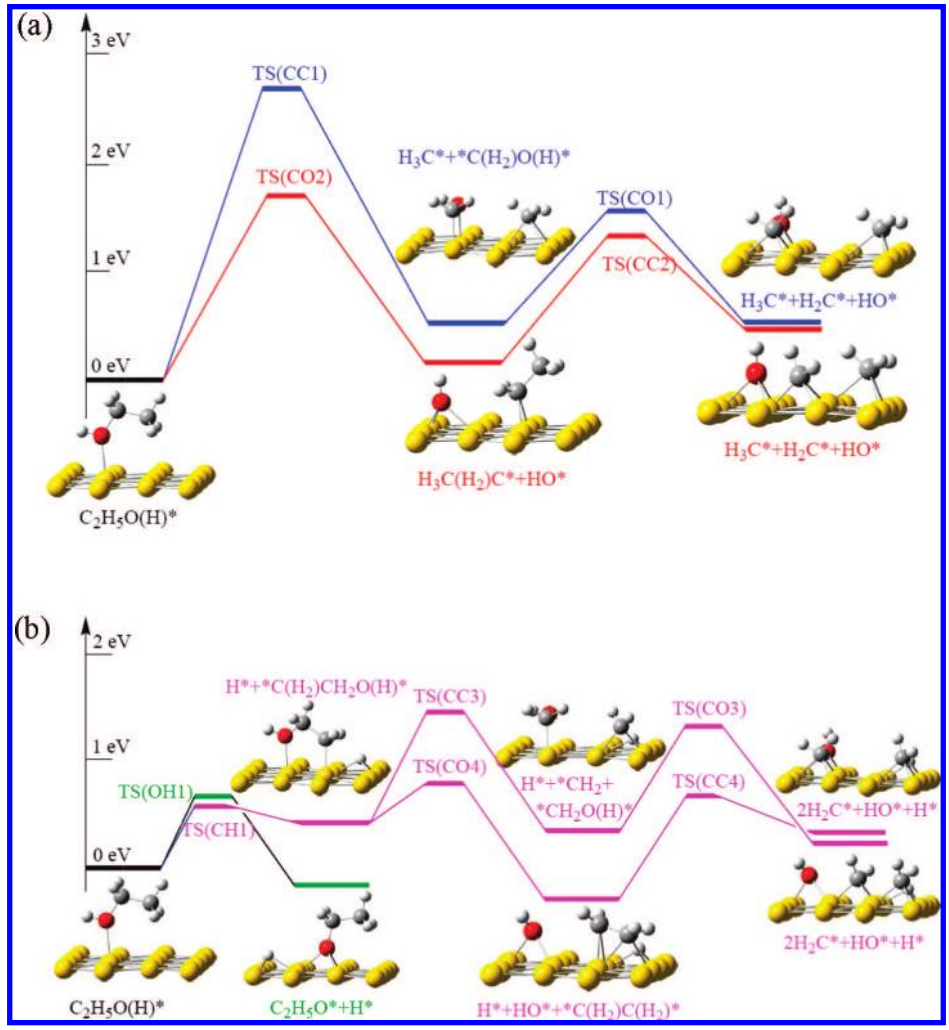

Figure 1. PES and geometrical structures of ethanol decomposition on Rh(111) surface. The initial (a) C−C and C−O and (b) C−H and O−H bond breaking processes in reactions 4−7, respectively (Table 1). The decompositions on other surfaces have similar results and are not shown.

$$C_2H_5O^* \xrightarrow{TS(CO6)} H_3C(H_2)C^* + O^* \xrightarrow{TS(CC6)} H_3C^* + H_2C^* + O^* \quad (9)$$

$$C_2H_5O^* \xrightarrow{TS(CH2)} {}^*C(H_2)C(H_2)O^* + H^* \rightarrow \begin{cases} \xrightarrow{TS(CC7)} H_2C^* + {}^*C(H_2)O^* + H^* \xrightarrow{TS(CO7)} 2H_2C^* + O^* + H^* \\ \xrightarrow{TS(CO8)} {}^*C(H_2)C(H_2)^* + O^* + H^* \xrightarrow{TS(CC8)} 2H_2C^* + O^* + H^* \end{cases} \quad (10)$$

Finally, the fragments of H_3C^* and HO^* from earlier dissociation processes can completely decompose to form atomic C*, O*, and H* adsorptions via reactions 11 and 12, respectively.

$$H_3C^* \xrightarrow{TS(CH3)} H_2C^* + H^* \xrightarrow{TS(CH4)} HC^* + 2H^* \xrightarrow{TS(CH5)} C^* + 3H^* \quad (11)$$

$$HO^* \xrightarrow{TS(OH2)} O^* + H^* \quad (12)$$

Comparing all the C−H bond breaking process, TS(CH3), TS(CH4), and TS(CH5) in the H_3C^* dissociation have lower barriers than TS(CH1) and TS(CH2) in the ethanol and $C_2H_5O^*$ dissociations, respectively. Comparing the C−H bond breaking processes in the H_3C^* dissociation, TS(CH5) has higher barrier than TS(CH3) and TS(CH4). This result can be related to the stable HC* adsorption with greater adsorption energies (−6.4 ∼ −3.6 eV) than those of H_2C^* (−4.3 ∼ −2.4 eV) and H_3C^* (−2.0 ∼ −1.4 eV) and is consistent with the recent works on Pt(111), Rh(111), Pd(111), and Ni(111) surfaces.[29−31] Although the TS(CH5) has a slightly higher dissociation barrier, HC* can react with O*, which is expected to be present on catalyst surfaces during the reforming process, lowering its C−H bond dissociation barrier.[29] The result implies that atomic C and H adsorptions can occur easily on the surfaces once the ethanol is decomposed to H_xC^*.

In the O−H bond breaking process, TS(OH2) exhibits a lower dissociate barrier than that of TS(OH1), which is close to the result of a recent calculation.[32] It might be a result of the electron-pushing C_2H_5 group stabilizing the $C_2H_5O^*$ fragment when the O−H bond is breaking in reaction 7.

Comparing different elementary steps of ethanol decomposition on the same metal surface, the initial C−C bond breaking process of the adsorbed ethanol and $C_2H_5O^*$ through TS(CC1) and TS(CC5), respectively, have relatively higher dissociation barriers than those of C−O [TS(CO2) or

TABLE 2: Dissociation Barriers and Heats of Reaction in Parentheses (eV) of the C_2H_5O−, H_3C−, and HO− Decomposition Processes on the Nine Metal (111) Surfaces

	Co	Rh	Ir	Ni	Pd	Pt	Cu	Ag	Au
Reaction 8: $C_2H_5O^* \xrightarrow{TS(CC5)} H_3C^* + {}^*C(H_2)O^* \xrightarrow{TS(CO5)} H_3C^* + H_2C^* + O^*$									
TS(CC5)	1.52(0.78)	1.41(0.65)	1.85(0.37)	1.62(1.26)	1.93(0.53)	2.08(1.04)	2.27(1.87)	3.79(1.66)	3.45(0.88)
TS(CO5)	0.78(-0.10)	1.12(-0.23)	1.01(-0.13)	1.13(-0.49)	1.63(0.75)	1.50(0.42)	1.70(1.48)	3.65(2.60)	2.86(2.32)
Reaction 9: $C_2H_5O^* \xrightarrow{TS(CO6)} H_3C(H_2)C^* + O^* \xrightarrow{TS(CC6)} H_3C^* + H_2C^* + O^*$									
TS(CO6)	0.86(0.12)	1.27(-0.07)	1.20(-0.13)	0.90(0.26)	1.27(0.42)	1.37(0.03)	1.83(1.03)	2.13(1.13)	1.57(1.40)
TS(CC6)	1.15(0.25)	1.43(0.36)	1.47(-0.01)	1.28(0.45)	1.43(0.82)	1.65(0.10)	1.86(1.20)	3.05(2.02)	2.71(1.64)
Reaction 10: $C_2H_5O^* \xrightarrow{TS(CH2)} {}^*C(H_2)C(H_2)O^* + H^* \rightarrow \begin{cases} \xrightarrow{TS(CC7)} H_2C^* + {}^*C(H_2)O^* + H^* \xrightarrow{TS(CO7)} 2H_2C^* + O^* + H^* \\ \xrightarrow{TS(CO8)} {}^*C(H_2)C(H_2)^* + O^* + H^* \xrightarrow{TS(CC8)} 2H_2C^* + O^* + H^* \end{cases}$									
TS(CH2)	1.28(1.08)	0.55(0.52)	0.44(0.04)	1.47(1.15)	1.03(0.55)	1.25(-0.27)	1.67(1.11)	3.12(1.35)	1.68(1.34)
TS(CC7)	0.19(-0.18)	0.45(-0.24)	0.72(-0.03)	0.30(-0.19)	0.60(-0.06)	0.73(0.18)	1.70(1.46)	2.30(1.02)	1.60(0.74)
TS(CO7)	0.10(-0.57)	0.07(-0.48)	0.50(-0.73)	0.12(-0.69)	0.71(-0.78)	1.14(0.43)	1.25(0.48)	3.55(2.55)	3.60(2.28)
TS(CO8)	0.05(-1.51)	0.05(-1.10)	0.21(-0.60)	0.10(-1.33)	0.18(-0.62)	1.02(0.24)	1.13(0.09)	2.02(-0.12)	1.24(0.36)
TS(CC8)	0.92(0.90)	0.97(0.84)	1.44(0.32)	1.05(1.01)	1.78(1.52)	1.40(0.48)	2.27(2.00)	4.10(3.81)	3.02(2.96)
Reaction 11: $H_3C^* \xrightarrow{TS(CH3)} H_2C^* + H^* \xrightarrow{TS(CH4)} HC^* + 2H^* \xrightarrow{TS(CH5)} C^* + 3H^*$									
TS(CH3)	0.11(-0.17)	0.18(-0.25)	0.28(0.04)	0.32(-0.20)	0.56(-0.07)	0.64(-0.01)	1.25(0.78)	2.03(1.69)	1.67(1.39)
TS(CH4)	0.15(-0.33)	0.11(-0.51)	0.31(-1.14)	0.17(-0.34)	0.33(-0.46)	0.54(-0.50)	1.05(0.61)	1.66(1.32)	1.21(0.77)
TS(CH5)	1.08(0.50)	1.07(0.42)	1.11(0.76)	1.24(0.60)	1.31(0.40)	1.16(0.61)	1.56(1.37)	2.27(1.90)	2.16(1.63)
Reaction 12: $HO^* \xrightarrow{TS(OH2)} O^* + H^*$									
TS(OH2)	0.99(-0.16)	1.35(-0.21)	1.45(-0.16)	1.00(-0.13)	1.26(0.15)	1.57(0.01)	1.82(0.71)	2.60(1.74)	2.06(1.40)
Dissociation barriers:	> 0.5	0.5 ~ 1.0	1.0 ~ 1.5	1.5 ~ 2.0	2.0 ~ 2.5	> 2.5 eV			

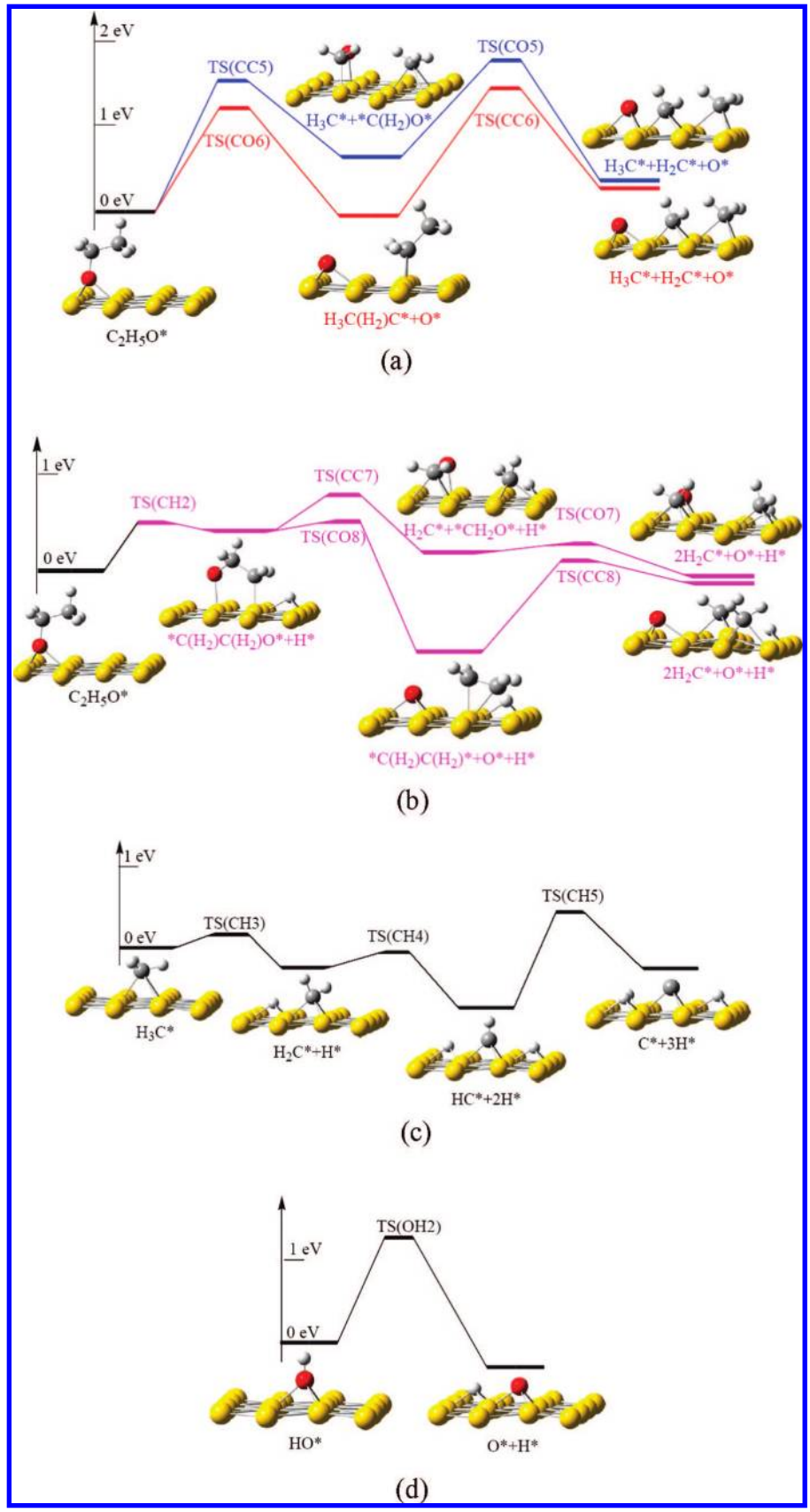

Figure 2. PES and geometrical structures of the fragment (C_2H_5O*, H_3C*, and HO*) decomposition on Rh(111) surface. The initial (a) C−C and C−O, of C_2H_5O*, (b) C−H of C_2H_5O*, (c) C−H of H_3C*, and (d) O−H of HO* bond breaking processes in reactions 8−12, respectively (Table 2). The decompositions on other surfaces have similar results and are not shown.

TS(CO6)], C−H [TS(CH1) or TS(CH2)], and O−H [TS(OH1)] bond breaking processes. The result indicates that ethanol decomposition through reactions 4 and 8 is less likely to occur; it is in good agreement with previous calculations on Pt(111) and Rh(111) surfaces.[8,12,28] Furthermore, comparing the initial bond dissociations of C−O (reactions 5 and 9)

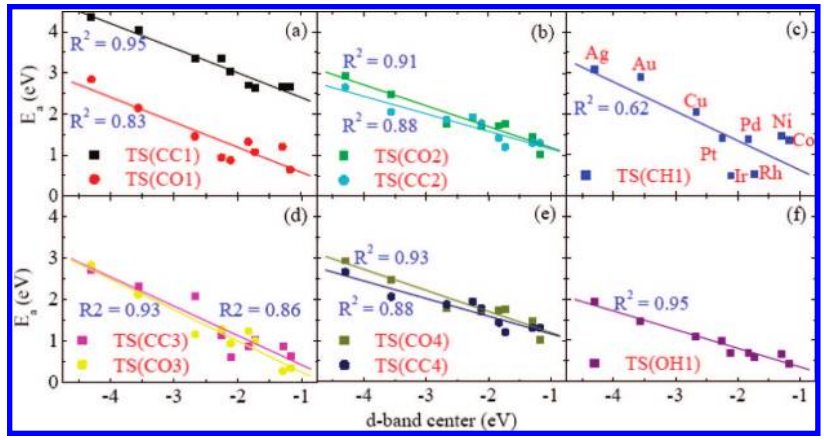

Figure 3. Plot of the dissociation barriers of ethanol decomposition in reactions 4−7 against the corresponding d-band centers of the nine selected metal (111) surfaces.

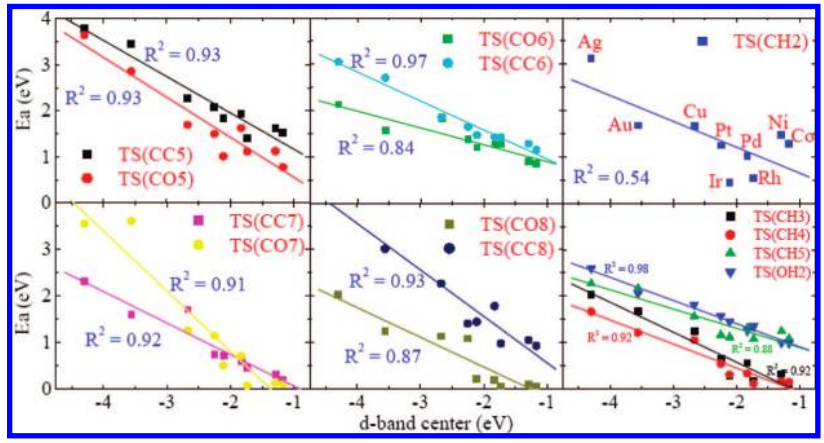

Figure 4. Plot of the dissociation barriers of the fragments (C_2H_5O−, H_3C− and HO−) decomposition in reactions 8−12 against the corresponding d-band centers of the nine selected metal (111) surfaces.

with the initial C−H (reactions 6 and 10) bond dissociations, the barriers of TS(CH1) and TS(CH2) on some metal surfaces are lower than these of TS(CO2) and TS(CO6), respectively. In addition, the following dissociation barriers in reaction 6 [TS(CC3), TS(CC4), TS(CO3), and TS(CO4)] and reaction 10 [TS(CC7), TS(CC8), TS(CO7), and TS(CO8)] are relatively smaller than those of TS(CC2) in reaction 5 and TS(CC6) in reaction 9, respectively. This result indicates that the decomposition paths are more likely through reactions 6 and 10 for the initial C−H bond dissociation. Finally, the low barrier of TS(OH1) implies that the C_2H_5O* intermediate is expected to be present during the decomposition and may follow similar dissociation routes as the $C_2H_5O(H)$* adsorbate.

Compare the same elementary step on different metal surfaces, the dissociation barriers in Tables 1 and 2 have been examined by the d-band theory,[23,26] in which the higher d-band center of the metal results in a lower dissociation barrier. As shown in Figures 3 and 4 (corresponding to Tables 1 and 2, respectively), most of the predicted dissociation barriers show a good linear correlation with the metal d-band centers, except those of TS(CH1) and TS(CH2) which have the lowest R^2 of 0.62 and 0.54, respectively. The linear relationship in Figures 3c and 4c breaks down due to Rh(111) and Ir(111) surfaces having the suitable bond distances of Rh−Rh (2.72 Å) and Ir−Ir (2.75 Å), respectively, to form a more stable five-member ring, −M−$C(H_2)$−$C(H_2)$−O(H)−M− or −M−$C(H_2)$−$C(H_2)$−O−M− (where M represents a surface metal atom) and to lower the barriers of TS(CH1) or TS(CH2), respectively. Therefore, the dissociation barriers of TS(CH1) and TS(CH2) will not only be affected by the d-band center (electronic effect) but also by the bond distance of surface metals (geometrical effect), even for metals with an identical crystal structure and surface orientation. This kind of geometrical effects only appear in the intermediates with double (or multiple) adsorptions on the surface, but may not be observed in the dissociation of small molecules, e.g. H_2, NO, O_2, or CH_4, with single adsorption as described in a previous calculation.[23]

Comparing current decomposition calculations with previous reforming experiments, the computed result predicts that reactions 6 and 10 are the most likely pathways for ethanol decomposition through the lower barriers of TS(CH1) and TS(CH2) forming the stable *$C(H_2)C(H_2)O(H)$* and *$C(H_2)C(H_2)O$* adsorbates, respectively; the result is in good agreement with the experimental observation that the doubly adsorbed five-member ring configurations are regarded as the key intermediates in the reaction.[33] In addition, the excellent performance of Rh- and Ir-based catalysts in the reforming experiments[2−5,34] can be attributed to the geometrical effect which results in the lowest TS(CH1) and TS(CH2) barriers on Rh(111) and Ir(111) surfaces. Furthermore, the computed high dissociation barriers for the (111) surface of group 11 elements (Cu, Ag, and Au; Tables 1 and 2) suggest poor catalytic properties for ethanol reforming and can well explain why these metals have infrequently been reported in the reforming experiments.[2−4]

The calculations on the (111) surface of group 9 metals (Co, Rh, and Ir) show low barriers to promote bond cleavages, which agrees well with the decomposition experiments.[35−37] However,

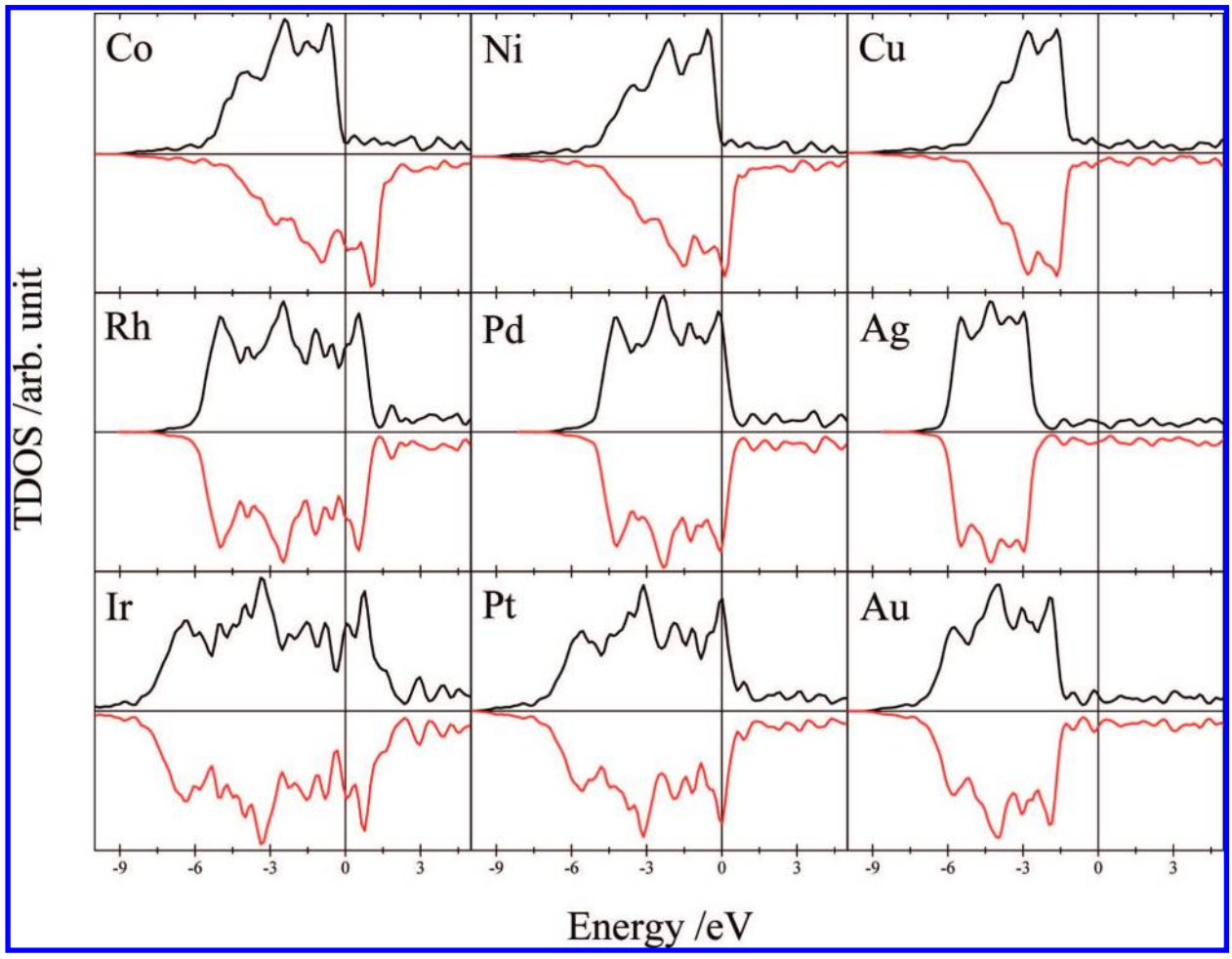

Figure 5. Total DOS of Co(111), Ni(111), Cu(111), Rh(111), Pd(111), Ag(111), Ir(111), Pt(111), and Au(111) surfaces.

it is not sufficient to clarify the results from the reforming experiments,[2−4] in which Rh-, Ir-, Pt-, and Pd-based catalysts show better conversion efficiencies than others. This inadequacy can be resolved by taking the redox capability of catalysts into consideration in the following electronic structure analysis.

The electronic structures of the selected metal surfaces have been examined from the density of state (DOS) analysis. Figure 5 shows the total DOS (mostly contributed from the metal d-band states) of spin α and spin β from group 9−11 metals with the same crystal structure and surface orientation. Comparing the DOS between 3d to 5d (row comparison in the periodic table), the upper 3d metals (Co, Ni, and Cu) have more contracted DOS distribution and the lower 5d metals (Ir, Pt, and Au) have more delocalized ones. Similarly, the distributions of the group 11 elements (Cu, Ag, and Au) are more contracted than the metals in groups 9 and 10 in the column comparison. The shapes of DOS, which can be attributed to the nuclear-electron attraction that the upper-right elements in the periodic table have stronger attraction and result in more contracted distributions, are closely related to the redox capability of catalytic metals. The delocalized DOS around the Fermi level, which can accept/donate electrons and act as electron reservoir in the redox reaction,[38] can be considered as an indicator of redox capability of catalysts. On the other hand, the empty/filled electronic states near the Fermi level can accept/donate more electrons to enhance the reduction/oxidation reactions. Since these metals are conductive elements, their DOS are all continuous around the Fermi level. However, the surfaces of Rh(111) and Ir(111) show a much higher DOS distribution near the Fermi level and can be regarded as the more active catalysts for redox reactions in the reforming of ethanol. Cu(111), Ag(111), and Au(111) surfaces, in contrast, are relatively less active.

Considering both the computed decomposition barriers and DOS distributions, the (111) surfaces of group 11 elements (Cu, Ag, and Au) are expected to be less efficient in the reforming of ethanol due to their high dissociation barriers and low DOS distributions near the Fermi level. On the other hand, Rh(111) and Ir(111) surfaces are anticipated to be the best ethanol reformers among these metals due to their low TS(CH1) and TS(CH2) barriers and high DOS distributions around the Fermi level. Furthermore, the better efficiency of Pt- and Pd-based reformers than Co- and Ni-based ones in the reforming experiments[3,39−42] can be understood from the slightly elevated barriers and the relative higher DOS distribution around the Fermi level on Pt(111) and Pd(111) than Co(111) and Ni(111) surfaces. This result may also indicate that the redox capability plays a more important role than decomposition does in ethanol reforming. In addition, though Co(111) and Ni(111) surfaces have lower barriers, but with insufficient redox capability the rapid dehydrogenation process results in carbon poisoning on catalyst surfaces.[23]

It is possible that metal oxides, such as CeO_2, ZrO_2, MgO, etc., in the practical metal−metal oxide reformers may change the electronic structures of the supported metals[43] and varies the catalytic ability of reformers. However, these metal oxides may cause a similar enhancement or deterioration of the catalytic

ability on supported metals.[42,44] Therefore, current mechanistic study on a series of pure metal surfaces is sufficient to clearly explain the efficiencies of catalysts in the reforming experiment. Furthermore, this bottom-up approach can provide a fundamental understanding of reforming mechanisms and the scientific underpinning for designing novel catalysts with better efficiencies.

4. Conclusion

In conclusion, the reforming mechanism for hydrogen conversion from ethanol has been extensively examined by both energetic calculation and electronic structure analysis. The ethanol decomposition reaction has been systematically elucidated by calculating the reaction barriers of all elementary C−C, C−O, C−H, and O−H bond breaking processes on the group 9−11 metals. The computed PES's show that the dissociation barriers for the (111) surfaces of Co, Ni, Rh, and Ir are lower than those on the same structured surfaces of Cu, Ag, and Au. Furthermore, among all the possible decomposition pathways, the initial C−H bond breaking processes forming $*C(H_2)C(H_2)O(H)*$ and $*C(H_2)C(H_2)O*$ adsorbates are considered to be the most effective routes with lower reaction barriers. According to the electronic structure analysis, the Rh(111) and Ir(111) surfaces are expected to have better redox capability than the other metal surfaces for their high DOS distribution near the Fermi level. Both the lower decomposition barriers and the superior redox capabilities are considered as the main reasons for the excellent conversion efficiencies of Rh- and Ir-based catalysts.

Acknowledgment. This work is supported by the National Science Council, Taiwan, (NSC97-2113-M-009-003-). We also want to acknowledge the support from ATU Plan of MOE, Taiwan. CPU time from Taiwan's National Center for High-performance Computing (NCHC) and the Institute of Nuclear Energy Research (INER) is greatly appreciated.

References and Notes

(1) Lubitz, W.; Tumas, W. *Chem. Rev.* **2007**, *107*, 3900.
(2) Haryanto, A.; Fernando, S.; Murali, N.; Adhikari, S. *Energy Fuels* **2005**, *19*, 2098.
(3) Navarro, R. M.; Pena, M. A.; Fierro, J. L. G. *Chem. Rev.* **2007**, *107*, 3952.
(4) Ni, M.; Leung, D. Y. C.; Leung, M. K. H. *Int. J. Hydrogen Energy* **2007**, *32*, 3238.
(5) Deluga, G. A.; Salge, J. R.; Schmidt, L. D.; Verykios, X. E. *Science* **2004**, *303*, 933.
(6) Lee, A. F.; Chang, Z.; Ellis, P.; Hackeet, S., F. J.; Wilson, K. *J. Phys. Chem. C* **2007**, *111*, 18844.
(7) Skoplyak, O.; Barteau, M. A.; Chen, J. G. *J. Phys. Chem. B* **2006**, *110*, 1686.
(8) Wang, H.-F.; Liu, Z.-P. *J. Phys. Chem. C* **2007**, *111*, 12157.
(9) Alcala, R.; Mavrikakis, M.; Dumesic, J. A. *J. Catal.* **2003**, *218*, 178.
(10) Xu, J. Z.; Zhang, X. P.; Zenobi, R.; Yoshinobu, J.; Xu, Z.; Yates, J. T., Jr. *Surf. Sci.* **1991**, *256*, 288.
(11) Lee, A. F.; Gawthrope, D. E.; Hart, N. J.; Wilson, K. *Surf. Sci.* **2004**, *548*, 200.
(12) Vesseli, E.; Baraldi, A.; Comelli, G.; Lizzit, S.; Rosei, R. *ChemPhysChem* **2004**, *5*, 1133.
(13) Yang, M.-M.; Bao, X.-H.; Li, W.-X. *J. Phys. Chem. C* **2007**, *111*, 7403.
(14) Fartaria, R. P. S.; Freitas, F. F. M.; Silva Frenandes, F. M. S. *Int. J. Quantum Chem.* **2007**, *107*, 2169.
(15) Kresse, G.; Hafner, J. *Phys. Rev. B* **1993**, *47*, 558.
(16) Kresse, G.; Hafner, J. *Phys. Rev. B* **1994**, *49*, 1425.
(17) Kresse, G.; Furthmüller, J. *Phys. Rev. B* **1996**, *54*, 11169.
(18) Cleperley, D. M.; Alder, B. J. *Phys. Rev. Lett.* **1980**, *45*, 566.
(19) Perdew, J. P.; Yang, Y. *Phys. Rev. B* **1992**, *45*, 244.
(20) Blöchl, P. E. *Phys. Rev. B* **1994**, *50*, 17953.
(21) Kresse, G.; Joubert, D. *Phys. Rev. B* **1999**, *59*, 1758.
(22) Monkhorst, H. J.; Pack, J. D. *Phys. Rev. B* **1976**, *13*, 5188.
(23) Hammer, B.; Norskov, J. K. *Adv. Catal.* **2000**, *45*, 71.
(24) Liu, Z.-P.; Hu, P. *J. Am. Chem. Soc.* **2003**, *125*, 1958.
(25) Cheng, J.; Gong, X.-Q.; Hua, P.; Lok, C. M.; Ellis, P.; French, S. *J. Catal.* **2008**, *254*, 285.
(26) Norskov, J. K.; Bligaard, T.; Hvolbak, B.; Abild-Pedersen, F.; Chorkendorff, I.; Christensen, C. H. *Chem. Soc. Rev.* **2008**, *37*, 2163.
(27) Mills, G.; Jonsson, H.; Schenter, G. K. *Surf. Sci.* **1995**, *324*, 305.
(28) Wang, H.-F.; Liu, Z.-P. *J. Am. Chem. Soc.* **2008**, *130*, 10996.
(29) Inderwildi, O. R.; Jenkins, S. J.; King, D. A. *Angew. Chem., Int. Ed.* **2008**, *47*, 5253.
(30) Inderwildi, O. R.; Jenkins, S. J.; King, D. A. *J. Am. Chem. Soc.* **2007**, *129*, 1751.
(31) Wang, S. G.; Liao, X. Y.; Hu, J.; Cao, D. B.; Li, Y. W.; Wang, J. G.; Jiao, H. J. *Surf. Sci.* **2007**, *601*, 1271.
(32) Gokhale, A. A.; Dumesic, J. A.; Mavrikakis, M. *J. Am. Chem. Soc.* **2008**, *130*, 1402.
(33) Sheng, P.-Y.; Yee, A.; Bowmaker, G. A.; Idriss, H. *J. Catal.* **2002**, *208*, 393.
(34) Cai, W.; Zhang, B.; Li, Y.; Xu, Y.; Shen, W. *Catal. Comm.* **2007**, *8*, 1588.
(35) Llorca, J.; Homs, N.; Sales, J.; de la Piscina, P. R. *J. Catal.* **2002**, *209*, 306.
(36) Sheng, P.-Y.; Idriss, H. *J. Vac. Sci. Technol. A* **2004**, *22*, 1652.
(37) Velu, S.; Satoh, N.; Gopinath, C. S.; Suzuki, K. *Catal. Lett.* **2002**, *82*, 145.
(38) Liu, Z.-P.; Jenkins, S. J.; King, D. A. *Phys. Rev. Lett.* **2005**, *94*, 196102.
(39) Breen, J. P.; Burch, R.; Coleman, H. M. *Appl. Catal., B* **2002**, *39*, 65.
(40) Erdohelyi, A.; Rasko, J.; Kecskes, T.; Toth, M.; Domok, M.; Baan, K. *Catal. Today* **2006**, *116*, 367.
(41) Fierro, V.; Akdim, O.; Mirodatos, C. *Green Chem.* **2003**, *5*, 20.
(42) Liguras, D. K.; Kondarides, D. I.; Verykios, X. E. *Appl. Catal., B* **2003**, *43*, 345.
(43) Xu, Y.; Greeley, J.; Mavrikakis, M. *J. Am. Chem. Soc.* **2005**, *127*, 12823.
(44) Aupretre, F.; Descorme, C.; Duprez, D. *Catal. Comm.* **2002**, *3*, 263.

JP810307H